The Journal of Chemical Physics

Infrared laser multiple-photon dissociation of $CTCl_3$: Wavelength dependence, collisional effects, and tritium/deuterium isotope selectivity

Cite as: J. Chem. Phys. **81**, 2363 (1984); https://doi.org/10.1063/1.447936
Submitted: 18 April 1984 • Accepted: 11 May 1984 • Published Online: 31 August 1998

Frank Magnotta and Irving P. Herman

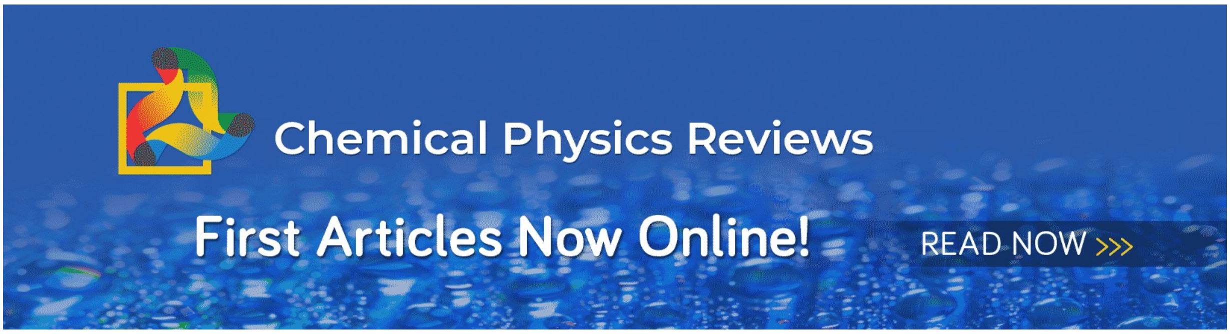

Infrared laser multiple-photon dissociation of $CTCl_3$: Wavelength dependence, collisional effects, and tritium/deuterium isotope selectivity

Frank Magnotta and Irving P. Herman
Department of Physics, University of California, Lawrence Livermore National Laboratory, Livermore, California 94550

(Received 18 April 1984; accepted 11 May 1984)

Isotopically selective infrared multiple-photon dissociation of $CTCl_3$ in $CDCl_3$ was investigated using a pulsed CO_2 laser-pumped NH_3 laser in the 12 μm region. The wavelength dependence of $CTCl_3$ MPD in the ν_4 absorption band was studied and the observed MPD peak was found to be shifted $\sim 10\ \mathrm{cm}^{-1}$ to the red of the absorption peak at 835 cm^{-1}, consistent with the anharmonicity of the $CTCl_3$ ν_4 mode. The $CTCl_3$ dissociation probability per pulse was investigated under various experimental conditions, including laser energy, pulse duration, and $CDCl_3$ and buffer gas pressure. A rate equation model was used to analyze the $CTCl_3$ experiments assuming various multiple-photon absorption and collisional relaxation mechanisms; this modeling effort was extended to a brief, more general, investigation of multiple-photon absorption by molecules with prespecified dissociation probability profiles. Lower limit single step T/D enrichment factors in chloroform MPD exceeding 15 000 were achieved under optimized conditions of the above parameters. No evidence of any $CDCl_3$ depletion or decomposition product was observed in irradiated 200 ppm $CTCl_3/CDCl_3$ mixtures. $CDCl_3$ absorption measurements were made using an optically pumped NH_3 laser, and the observed high fluence T/D optical selectivity was found to be sufficiently high for practical tritium recovery.

INTRODUCTION

The use of D_2O as coolant and moderator in heavy-water nuclear reactors results in production of tritiated water and, therefore, radioactive contamination. Interest in developing technologies for removing tritiated water stems not only from health hazard conditions, but also from the subsequent use of tritium as fuel in fusion reactors. We reported[1] the first successful laser-assisted T/D separation in which isotopically selective multiple-photon dissociation (MPD) of $CTCl_3$ in a background of $CDCl_3$ was achieved using a CO_2 laser-pumped NH_3 laser at 12.08 μm. TCl was the tritium-bearing product of interest in these experiments. More recently, Makide *et al.*[2] reported T/D separation using C_2TF_5 photolyzed by short pulse (100 ns) CO_2 laser radiation, with separation factors exceeding 3000 at -78 °C with 10 Torr deutero-pentafluoroethane pressure. Since our earlier preliminary set of experiments, the experimental precision has been significantly upgraded. In this paper a lower limit separation factor exceeding 15 000 at room temperature (significantly greater than the earlier value of 165[1]) is reported, again using $CTCl_3$ photolysis at 12.08 μ.

In addition to the more precise value of the chloroform T/D enrichment factor, a refined determination of the $CTCl_3/CDCl_3$ isotopic absorption selectivity was made, and the dependence of the $CTCl_3$ MPD probability on laser frequency, fluence, and pulse width, and on added buffer gas was investigated. The dependence of MPD on molecular absorption and collisions was further studied using an energy-grained master equation model. Some general conclusions concerning multiple-photon absorption in $CTCl_3$ and other molecules were drawn from this study. Furthermore, several experiments were conducted to differentiate between resonant 12μ $CDCl_3$ decomposition due to the "collision-free," laser absorption process:

$$\begin{aligned} CTCl_3 + nh\nu \ &\rightarrow CTCl_3^{\dagger\dagger} && (1a)\\ &\rightarrow :CCl_2 + TCl \quad (>99\%)^3 && (1b)\\ &\rightarrow \cdot CTCl_2 + Cl \quad (<1\%)^3, && (1c)\\ CDCl_3 + nh\nu \ &\rightarrow :CCl_2 + DCl, && (2) \end{aligned}$$

and decomposition in which $CDCl_3/CTCl_3$ collisions are important, such as $CDCl_3$ reactions with either excited and unreacted tritiated chloroform

$$\begin{aligned} CDCl_3 + CTCl_3^{\dagger\dagger} \ &\rightarrow CDCl_3^{\dagger} + CTCl_3^{\dagger}, && (3)\\ CDCl_3^{\dagger} + nh\nu \ &\rightarrow :CCl_2 + DCl, && (4) \end{aligned}$$

or with $CTCl_3$ (and possibly $CDCl_3$) reaction products, e.g.,

$$CDCl_3 + :CCl_2 \rightarrow \text{products}. \qquad (5)$$

EXPERIMENTAL PROCEDURE

$CTCl_3$ was synthesized by base-catalyzed (OD^-) aqueous exchange between $CDCl_3$ and T_2O as described previously.[1] Samples containing T/D fractions $\eta \sim 200$ ppm were prepared by dilution in a grease-free, all stainless steel vacuum line immediately following synthesis to avoid radiolysis in high specific activity mixtures. Such samples proved to be stable for long periods (several months) displaying no observable ($<0.1\%$) impurity buildup by gas chromatograph analysis.

The experimental arrangement is depicted in Fig. 1. The gas handling system consisted of glassware and glass plug (*O* ring) stopcocks connected to an all stainless steel (*O*-ring free) reaction cell/transfer line maintained at $\lesssim 2 \times 10^{-7}$ Torr. The metal reaction cell (8 cm long, ~ 11 cc volume) was fitted with KCl Brewster angle windows and was connected to a heated transfer line via metal seat hermetically sealed Nupro bellows valves. After photolysis, unphotolyzed reactants and products were cryogenically transferred to the gas sampling valve loop of a temperature-pro-

J. Chem. Phys. 81 (5), 1 September 1984 0021-9606/84/172363-12$02.10

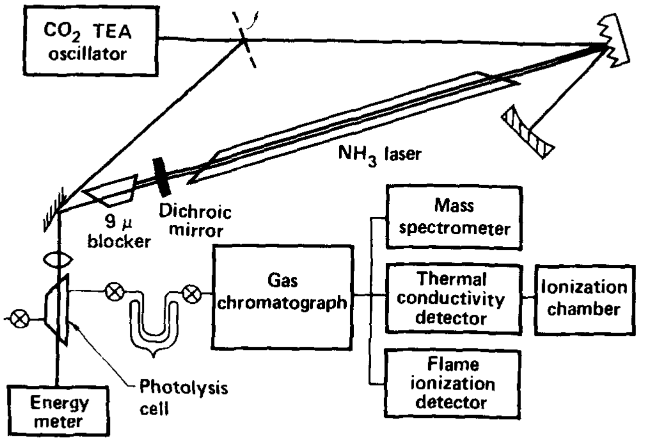

FIG. 1. Composite experimental apparatus.

grammed gas chromatograph. Following a trap cycle, the loop was heated to the temperature of the transfer lines prior to a helium flush to the gas chromatograph. A 6 foot long *n* octane on porasil-*c* column was used for separation. The effluent from the thermal conductivity detector of the gas chromatograph was directly coupled to a 250 cm^3 ionization chamber. The use of a heated metal, totally organic-free photolysis sampling system and following a carefully timed transfer sequence resulted in a significant improvement in run-to-run detection precision from $\pm$ 3%–5% as reported previously[1] to $\pm$ 0.2%. The additional attention given to system design is predicated by the "sticky" nature of highly chlorinated compounds. Depletion of CTCl$_3$ was monitored by a decrease in the ionization chamber signal, while changes in CDCl$_3$ concentration prior to and following photolysis were monitored (to $\pm$ 0.2%) by the thermal conductivity detector. Periodically during tritium depletion runs, blank runs using only neat CDCl$_3$ were made to assure there was no tritium pickup or exchange during transfer through the system.

A 0.3 Hz repetition rate, pulsed CO$_2$ laser (Lumonics 102-3) delivering 4 J at *R* (30), 9.22 μm in an 80 ns FWHM pulse ($\sim$ 1 μs tail) was used to optically pump an ammonia laser, as shown in Fig. 1. (At this low repetition rate, diffusional mixing in the photolysis cell between laser pulses is assured even at 50 Torr total pressure; the rms displacement is $\sim$3 cm). The ammonia resonator consisted of a 100 line/mm grating, a 120 cm long KCl Brewster angle gas cell, a partially reflective output coupler (97% *R* at 9.22 μm, 56% *T* at 12.08 μm) and a 6 m radius-of-curvature, totally reflecting copper tuning mirror. Coupling the CO$_2$ laser from the grating into the cavity allowed a two pass optical pumping configuration, and the dichroic output coupler facilitated easy wavelength tuning. Residual CO$_2$ pump radiation leaking through the output coupler was totally blocked by a 4 cm long gas cell containing 24 Torr CF$_3$I and 450 Torr SF$_6$. The ammonia laser pulse width was varied between 250 ns and 2 μs by controlling the NH$_3$: N$_2$ mixing ratio and total pressure, thereby partitioning varying amounts of NH$_3$ lasing to occur during the initial CO$_2$ laser "spike" and the "tail."[4] The spatial profile of the laser beam was obtained by scanning a 100 μm diam pinhole/pyroelectric detector assembly across the focused profile along several longitudinal and vertical slices of the beam. Near the focal region, the beam was somewhat elliptical (due to the NH$_3$ laser pumping arrangement), but was well characterized by a constant area vs fluence profile for fluences from zero to the peak.[5] The ammonia laser typically operated with output pulses of 250–500 mJ over the wavelength region of the $\nu_4 \leftarrow 0$ absorption in CTCl$_3$ (814–848 cm^{-1}). A 50 cm focal length KCl lens was used to focus the beam into the photolysis cell; with $\sim$400 mJ/cm^2 incident, there was a fluence of $\sim$16 J/cm^2 at the focus. In some experiments the photolyzing fluence was increased by more than a factor of two by retroreflecting the transmitted beam with a totally reflecting concave mirror approximately matching the focal length of the lens. The greater than double enhancement in fluence resulted from coupling part of the radiation back to the cavity, allowing multiple passages of light from the NH$_3$ laser dichroic output mirror. (Since the NH$_3$ output pulse energy was found to be fairly insensitive to the reflectivity of the output mirror, this feedback only weakly affected the laser operating parameters.) The beam profile from such "high fluence" experiments was not characterized via the pinhole techniques. The average energy per pulse was continuously measured either by transmission through the photolysis cell or by reflection from a beam splitter using a Gen-Tec Joulemeter coupled to a voltage-to-frequency converter/counter.

CDCl$_3$ absorption measurements were made by passing 12.08 μ radiation from the optically pumped NH$_3$ laser through a 198 cm long cell containing 20–200 Torr of CDCl$_3$. The input laser beam (partially reflected off a beam splitter) and transmitted beam pulse energies were simultaneously monitored using two Scientech energy meters and displayed on a *x*–*y* recorder. Data was calibrated by absorption null runs, during which the CDCl$_3$ was frozen out. The average incident fluence was $\sim$15 mJ/cm^2.

RESULTS AND DISCUSSION

Frequency dependence of CTCl$_3$ photolysis

The frequency dependence of CTCl$_3$ MPD was determined over the $\nu_4 \leftarrow 0$ absorption profile at discrete wave-

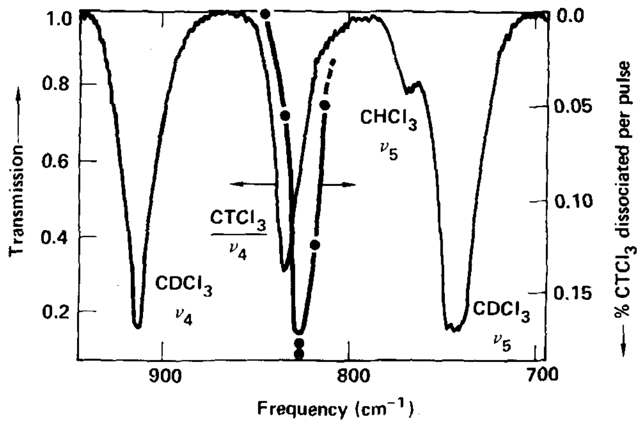

FIG. 2. The single frequency MPD profile of CTCl$_3$ (right axis; 275 mJ, 50 cm focal length lens, 200 mTorr, 202 ppm T/D) plotted alongside the small-signal transmission curve of a CTCl$_3$/CDCl$_3$ mixture (CDCl$_3$:ν_4 at 914 cm^{-1}, ν_5 near 747 cm^{-1}, CTCl$_3$:ν_4 at 835 cm^{-1}).

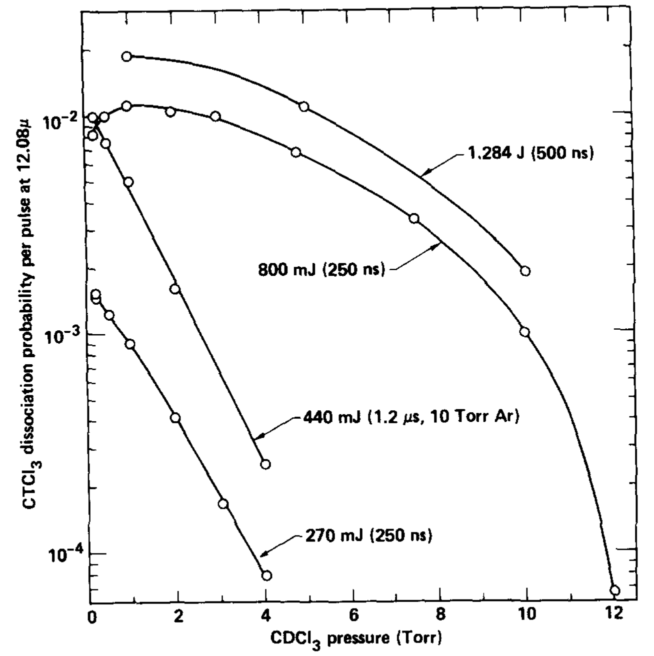

FIG. 3. The CTCl$_3$ dissociation probability per pulse (normalized to the cell volume) vs added CDCl$_3$ pressure for a variety of conditions [short pulse (250 ns) at 270 mJ (198 ppm T/D) and 800 mJ (multiple retroreflection; 198 ppm T/D under 5 Torr, 32 ppm T/D at 5 Torr and above); intermediate pulse length (500 ns) at 1.284 J (multiple retroreflection; 32 ppm T/D); and long pulse (1.2 μs) with 10 Torr argon at 440 mJ per pulse (198 ppm T/D; 12.08 μ)].

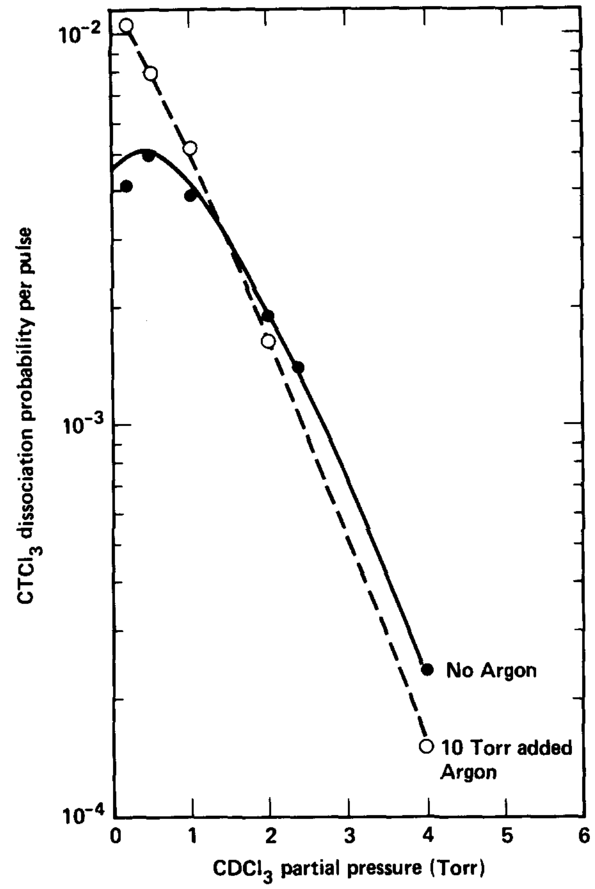

FIG. 4. The CTCl$_3$ MPD probability plotted vs CDCl$_3$ partial pressure with or without added argon (198 ppm T/D; 12.08 μ, 440 mJ, 1.2 μs). The smooth curve through the data points with no argon is fit with the model described in the text.

lengths of the ammonia laser across this range. Figure 2 shows the CTCl$_3$ absorption band of interest ($\nu_4 \leftarrow 0$) flanked by two CDCl$_3$ absorptions ($\nu_4, \nu_5 \leftarrow 0$), upon which is superimposed the MPD profile of CTCl$_3$ (right axis; 275 mJ, 50 cm focal length lens, 200 mTorr, 202 ppm T/D). The peak of the single frequency MPD profile is near 825 cm^{-1}, very close to the 12.08 μ, 828 cm^{-1} line of the ammonia laser. This MPD peak is shifted ~10 cm^{-1} to the red of the $\nu_4 \leftarrow 0$ absorption peak (835 cm^{-1}), a frequency shift which is comparable to the anharmonicity in the ν_4 CTCl$_3$ mode ($X_{44} = -8.9$ cm^{-1}),[1] estimated using Dennison's isotope shifting rule[6] and X_{44} measured in CDCl$_3$.[7] The 1ν MPD profile and $\nu_4 \leftarrow 0$ absorption profile have about the same width of ~16 cm^{-1}. In subsequent studies the laser wavelength was fixed at 12.08 μ.

Pressure and fluence dependence of the dissociation probability

A set of survey experiments was conducted to characterize the dependence of the dissociation yield of CTCl$_3$ MPD on fluence, pulse width, and pressure of added CDCl$_3$ or buffer gas. Figure 3 shows the yield per pulse vs CDCl$_3$ pressure for a number of fluences and 12 μ (FWHM) pulse widths.

A small multiple-photon absorption (MPA) bottleneck is evidenced by the slight upturn in the yield vs pressure as the CDCl$_3$ partial pressure is increased from zero in the 800 mJ run, shown in Fig. 3, as well as in the 440 mJ run (Fig. 4). At higher pressures, vibrational energy imparted to CTCl$_3$ is collisionally transferred to CDCl$_3$ and the CTCl$_3$ dissociation probability decreases. With higher fluences, excitation up the vibrational ladder is quite rapid and more easily overcomes the effect of deactivating collisions during the pulse duration. In Fig. 5 fundamentally the same collisional behavior is observed when helium, argon, or xenon is used as the buffer gas. For a given chloroform pressure, the peak dissociation probability with each buffer is about 2.4 times that of the neat sample. This suggests that in collision-free MPD of CTCl$_3$ fewer than 0.4 of available molecules are sufficiently resonant to undergo multiple-photon excitation at a laser fluence of ~16 J/cm^2 and intensity of ~1.3×10^7 W/cm^2.

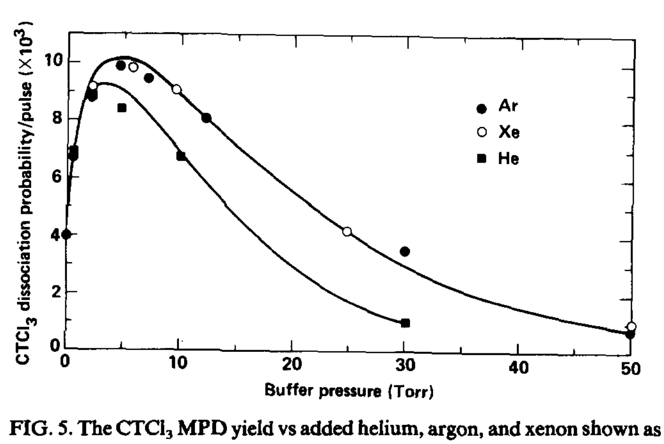

FIG. 5. The CTCl$_3$ MPD yield vs added helium, argon, and xenon shown as data points (200 ppm T/D, 200 mTorr chloroform; 12.08 μ, 410 mJ, 1.2 μs pulse width). The smooth curves represent best fit results based on rate equation model, described in the text.

An energy-grained master equation model of MPD, similar to that of Barker,[8] was briefly presented in Ref. 5 and applied to $CTCl_3$. This model includes only single quantum, incoherently pumped transitions. In Ref. 5, the dependence of the $CTCl_3$ multiple-photon dissociation probability on laser fluence was calculated with and without 10 Torr argon added, employing the measured depletion fractions and the laser spatial profile in this model. With 10 Torr of argon, 80% local dissociation probability was found to occur at a local laser fluence of ~ 16 J/cm^2, while 90% dissociation required ~ 18 J/cm^2. From Fig. 5, operation at the argon buffer pressure of 5 Torr is best (resulting in a slightly reduced fluence operation requirement).

The master equation model is further developed here and is again applied to $CTCl_3$, to help estimate the molecule-averaged collision cross sections from the data in Figs. 4 and 5. In this model, molecular vibrational structure is collapsed into a single vibrational ladder extending from $v = 0$ to the highest bound vibrational level v_d ($v_d = 26$ in $CTCl_3$ with 828 cm^{-1} level spacing), and then beyond into the dissociation continuum; each level has a population $n(v)$. The vibrational level degeneracy, $g(v)$, is determined by the Whitten-Rabinovitch model,[9] except for setting $g(v = 0-2) = 1$. For $v > v_d$, the molecule unimolecularly decays with a rate constant $k_{\rm uni}(v)$ given by RRKM theory.[3]

In general, the $v+1 \leftarrow v$ absorption cross section, $\sigma(v,\omega)$, can be modeled by a profile whose center frequency and width are parametrized by v and the laser frequency ω. Since the data under consideration were obtained only with the resonant 828 cm^{-1} ammonia laser line, the energy level spacing in the model is set equal to 828 cm^{-1}, and σ is simplified to $\sigma(v)$. One general form for the absorption cross section[8] is

$$\sigma(v) = a(v+1)^b. \tag{6}$$

Since small compensating adjustments in a and b can produce roughly identical dissociation probability profiles,[5] initially b is removed as an adjustable parameter here, and is set equal to zero,[10] which is the value for the best fit case in Ref. 5. As detailed below, the effects of rotational and vibrational state-changing collisions are incorporated into these rate equations, consistent with the spirit of this model, by using suitably averaged collision cross sections. A Gear[11] numerical integration computer code is used to solve the rate equations for a given reaction mixture and laser temporal profile (assumed to be a square pulse here). The calculated dissociation probabilities are then convoluted with the experimentally determined laser fluence and intensity distribution for comparison with experimental results.

Power broadening is usually much smaller than both vibrational transition profile widths and excited level anharmonic shifts under the conditions of most MPD experiments. Consequently, because of the seeming lack of suitable absorption resonances in most polyatomics, it is surprising that a large fraction of all irradiated molecules is observed to undergo multiple-photon absorption and dissociation under usual conditions. Most likely, the molecule experiences a complex series of rotational level changes in the lowest vibrational levels via a succession of absorption and then emission steps. This has been proposed by Platonenko,[12] and has been further discussed by Fuss and Kompa.[13] Additionally, Ruhman and Haas[10] have examined the influence of rotational structure in multiple-photon excitation, using a set of rate equations including individual vibrational-rotational transitions to describe a molecule with either no or total externally induced rotational relaxation. Still, this radiation-induced approach to rotational level equilibrium is usually incomplete. Therefore, not unexpectedly, the addition of an inert buffer gas to the neat resonant absorber has been found to substantially increase the MPD probability in many molecules[14] (including $CTCl_3$ here) by transferring nonresonant molecules to laser-depleted resonant states during the laser pulse. In effect, these collisions help to remove the multiple-photon absorption (MPA) "rotational-level bottleneck." This mechanism is incorporated into the present model by identifying a ground state reservoir of resonant states, with total population $n^r(0)$ and degeneracy $g^r(0)$, that is collisionally coupled to the remaining nonresonant states, characterized by $n^{\rm nr}(0)$ and $g^{\rm nr}(0)$, via rotational state-changing collisions with rate constant $k_{\rm rot}$. In equilibrium, $n^r(0)/n^{\rm nr}(0) = g^r(0)/g^{\rm nr}(0)$, and also $n(0) = n^r(0) + n^{\rm nr}(0)$ and $g(0) = g^r(0) + g^{\rm nr}(0)$. The fraction of resonant $v = 0$ states is $x_F = g^r(0)/g(0)$.

Vibrational relaxation in highly excited polyatomic molecules is currently under study by a variety of techniques.[15-17] As yet, there is no satisfactory theory or predictive model general enough to apply here. In this treatment, molecules are assumed to vibrationally relax one quantum down the ladder (from v to $v-1$) per effective collision, with a rate constant $k_{\rm vib}(v)$. Initially, $k_{\rm vib}$ is assumed to be independent of v, though this may not be strictly true at the lowest v.[18]

With a laser pulse of intensity $I(t)$ and frequency ω incident on an ensemble of resonant molecules interacting with a collision partner with a density n_c, the following rate equations describe excitation and dissociation:

$$\begin{aligned}\frac{dn^r(0)}{dt} = {} & \frac{\sigma(0)I}{\hbar\omega}\left[\frac{g(0)}{g(1)}n(1) - n^r(0)\right] \\ & + k_{\rm rot}n_c\{x_F[n^r(0)+n^{\rm nr}(0)] - n^r(0)\} \\ & + k_{\rm vib}n_c n(1),\end{aligned} \tag{7}$$

$$\frac{dn^{\rm nr}(0)}{dt} = k_{\rm rot}n_c\{(1-x_F)[n^r(0)+n^{\rm nr}(0)] - n^{\rm nr}(0)\}, \tag{8}$$

$$\begin{aligned}\frac{dn(v)}{dt} = {} & \frac{\sigma(v-1)I}{\hbar\omega}\left[n(v-1) - \frac{g(v-1)}{g(v)}n(v)\right] \\ & + \frac{\sigma(v)I}{\hbar\omega}\left[\frac{g(v)}{g(v+1)}n(v+1) - n(v)\right] \\ & + n_c\,[k_{\rm vib}(v+1)n(v+1) - k_{\rm vib}(v)n(v)] \\ & - k_{\rm uni}(v)n(v) \quad \text{for } v > 0.\end{aligned} \tag{9}$$

Here, $k_{\rm vib}(v) = k_{\rm vib}$ and $\sigma(v) = \sigma$. Also, $k_{\rm uni}(v)$ is the unimolecular reaction rate constant, which $= 0$ for $v \leqslant v_d$. Note that in the first term on the right side of Eq. (7), the total ground state density of states $g(0)$ is used instead of that for the resonant reservoir $g^r(0) = x_F g(0)$, because (to first order) the same ensemble of rotational states excited from $v = 1 \leftarrow 0$ will continue to be excited up the ladder. (Clearly, because of rotational state quantum number changes and new resonance conditions this is not strictly true; however, the use of x_F for $v = 0$ is meant to lump all these effects together.)

Using the laser spatial profiles measured in Ref. 5 with a scanning pinhole-detector arrangement, the data in Fig. 5 was fit using Eqs. (7)–(9). The results are shown as the solid curves in this figure. A satisfactory fit was obtained with $a = 1.7 \times 10^{-19}$ cm^2 and $b = 0$. The fraction of resonant ground vibrational level states is $x_F = 0.22$. For comparison, based on power broadening arguments one would expect $x_F \sim 0.04$. (These model-derived parameters are slightly different from those found in Ref. 5.)

From the model fit, $k_{\rm rot}$ is $\sim 1.2 \times 10^{-10}$ cm^3/molecule s (300 K) for He, Ar, and Xe. Using $k_{\rm rot} = \sigma_{\rm rot} < v_{\rm relative} >$, the ensemble-averaged rotational collision cross sections for CTCl$_3$-rare gas atom collisions are ~ 9.4, 26, and 38 Å^2, for He, Ar, and Xe, respectively. Since these cross sections are only somewhat smaller than gas kinetic (52, 62, 71 Å^2 for He, Ar, Xe/CTCl$_3$ collisions using diameters of 2.6,[19] 3.4,[19] 4.0,[19] and 5.5 Å[20] for He, Ar, Xe, and chloroform, respectively), the quantum number differences are small for collisionally coupled rotational states in the resonant and nonresonant reservoirs.

Similarly from the model fit, $k_{\rm vib} \sim 2.5 \times 10^{-11}$ cm^3/molecule s for Ar and Xe, and $\sim 3.8 \times 10^{-11}$ cm^3/molecule s for He, where $k_{\rm vib}$ represents the rate constant for the loss of an 828 cm^{-1} quantum by V-T relaxation. This corresponds to $\sigma_{\rm vib}$ of ~ 3.0, 5.4, and 7.9 Å^2 for He, Ar, and Xe, respectively ($k_{\rm vib} = \sigma_{\rm vib} < v_{\rm relative} >$) or CTCl$_3$ vibrational energy loss of ~ 50, 70, and 90 cm^{-1} per encounter with He, Ar, and Xe ($= 828$ cm$^{-1} \times \sigma_{\rm vib}/\sigma_{\rm gas\ kinetic}$).

Extension of this analysis to Fig. 4, in which CDCl$_3$ is the added gas, leads to $k_{\rm rot} \sim 1.2 \times 10^{-10}$ cm^3/molecule s ($\sigma_{\rm rot} \sim 37$ Å^2) and $k_{\rm vib} \sim 4.1 \times 10^{-10}$ cm^3/molecule s, ($\sigma_{\rm vib} \sim 125$ Å^2) or ~ 1100 cm^{-1} lost per CTCl$_3$–CDCl$_3$ collision. The curve drawn through the data with no added argon in Fig. 4 is this fit.

Clearly, due to the energy-grained nature of this model and the various approximations employed here, these results are molecule-averaged values. Though the assumptions that $k_{\rm vib}(v)$ and $\sigma(v)$ are independent of v leads to a good fit, it is certainly not a unique fit. Therefore, alternate absorption and collisional transfer models were briefly examined. They are summarized in the upper portion of Table I. Model A1 represents the original absorption and collisional cases described above.

Instead of assuming constant absorption cross section in the vibrational ladder ($b = 0$), in the alternate absorption model the $v = 1 \leftarrow 0$ absorption cross section was set equal to the CTCl$_3$ ground state value at 828 cm^{-1}, $a = 1.6 \times 10^{-18}$ cm^2,[1] and the ground state resonant fraction was kept fixed, $x_F = 0.22$. An adequate fit was obtained with $b = -0.79$ in Eq. (6), and values for the two collision rate constants were only slightly changed when compared to those in the original absorption model. For the argon/xenon data in Fig. 5, $k_{\rm rot}$ is lowered to $\sim 9.0 \times 10^{-11}$ cm^3/molecule s and $k_{\rm vib}$ increased by $\sim 10\%$ to $\sim 2.8 \times 10^{-11}$ cm^3/molecule s for this model A2.

The alternate collision model entails a variation in cross section proportional to either molecular energy or v, since a harmonic vibrational ladder is assumed here. So $k_{\rm vib}(v) = c(v/v_d)^d$ with $d = 1$, where $c = k_{\rm vib}(v_d)$ is the value at the dissociation energy. Some experimental evidence suggests that such a model well describes V-T transfer from "large" molecules (azulene[16]) to rare gas atoms. However, for V-T/V–V transfer to large molecules, a constant cross section, perhaps with a small added linear component,[16] is probably a more realistic model. Using the original $b = 0$ absorption model (with the original values for a, x_F, and $k_{\rm rot}$), a very good fit to the experimental curve was obtained with $k_{\rm vib}(v_d) \sim 1.6 \times$ the "$k_{\rm vib}$ = constant" value for each the Ar/Xe, He, and CDCl$_3$ collision partner case (model A3). This value of $k_{\rm vib}(v_d)$ is approximately equal to the $\sim 2\times$ change naively expected from averaging $k_{\rm vib}(v)$ over v with no weighting. Using this alternate collisional model (A3), highly excited CTCl$_3$ ($v \sim v_d$) suffers a V-T loss of ~ 80 cm^{-1}/He, ~ 100 cm^{-1}/Ar, ~ 140 cm^{-1}/Xe per collision with a rare gas atom. Extension of this alternate collision

TABLE I. Model conditions for Ar/Xe added buffer.

	$a^{\rm a}$ (10^{-19} cm^2)	$b^{\rm a}$	$c^{\rm b}$ (10^{-11} cm^3/molecule s)	$d^{\rm b}$	$k_{\rm rot}$ (10^{-11} cm^3/molecule s)
Experimental fit to CTCl$_3$ data ($x_F = 0.22$)$^{\rm c}$					
A1	1.7*	0	2.5*	0	12*
A2	16	−0.79*	2.8*	0	9*
A3	1.7*	0	4.0*	1	12*
A4	16	−0.79*	3.5*	1	9*
General model survey ($x_F = 1.0$; fast quenching)$^{\rm c}$					
B1	7.6*	−0.75	1.7*	−0.75	...
B2	67*	−1.5	1.9*	−0.75	...
B3	7.6*	−0.75	2.4*	0	...
B4	7.6*	−0.75	3.0*	+0.75	...
B5	67*	−1.5	3.1*	+1.5	...
B6	1.0*	0	2.5*	0	...
B7	0.18*	+0.75	5.5*	+0.75	...

[a] For absorption: $\sigma(v) = a(v+1)^b$ [Eq. (6)].

[b] For vibrational relaxation: $k_{\rm vib} = c(v/v_d)^d$ (see the text).

[c] * denotes a varied parameter.

model to $CTCl_3/CDCl_3$ V-T/V-V transfer is probably not meaningful because in this case cross sections at low v should be larger than this model predicts, as stated above.

Applying both this alternate collision model $[(k_{vib}(v) \propto v]$ and the alternate absorption model (case A4 in Table I, top), a satisfactory fit was obtained by changing $k_{vib}(v_d)$ to $\sim 1.25\times$ the "k_{vib} = constant" (A2) value. Therefore for each model variation (A1–A4), the value of $k_{vib}(v_d)$ is substantially the same (within $\sim \pm 25\%$ of the average of the A1–A4 rate constants).

With proper selection of parameters, each of these four models simulates the cell-averaged dissociation probability well. However, with these same parameters each model predicts a distinctive profile of $CTCl_3$ photon absorption vs added buffer pressure. These predictions are briefly described here for the case of added argon or xenon. Because of the procedural necessity of low $CTCl_3$ density in these studies, no corresponding experimental investigation of multiple-photon absorption was performed here to test these predictions.

The average number of quanta absorbed per molecule undergoing multiple-photon excitation is extracted in this model from the final state distribution, the state distribution of dissociating molecules, and the cumulative loss of molecular energy in collisions. In Fig. 6, this simulated photon absorption per $CTCl_3$ molecule is plotted vs added argon/xenon pressure at 6 and 16 J/cm^2 local fluence for each of the four parametrized models (A1–A4, Table I). [Because of the additional complication of rotational relaxation at very low pressure ($\leqslant$3 Torr), the presented curves begin at 3 Torr.] As a point of reference, at local fluences of 6 and 16 J/cm^2 the dissociation probability is calculated to be $\sim$0.03 and $\sim$0.66, respectively. Though the parameters for each model were selected to simulate the same observed cell-averaged dissociation probability data, the displayed local fluence curves in Fig. 6, as well as the respective cell-averaged curves (not shown here), are different for each model. These observations should help select the proper (incoherent) absorption/collision model in general studies, when multiple-photon absorption measurements are made in association with analyzed dissociation data.

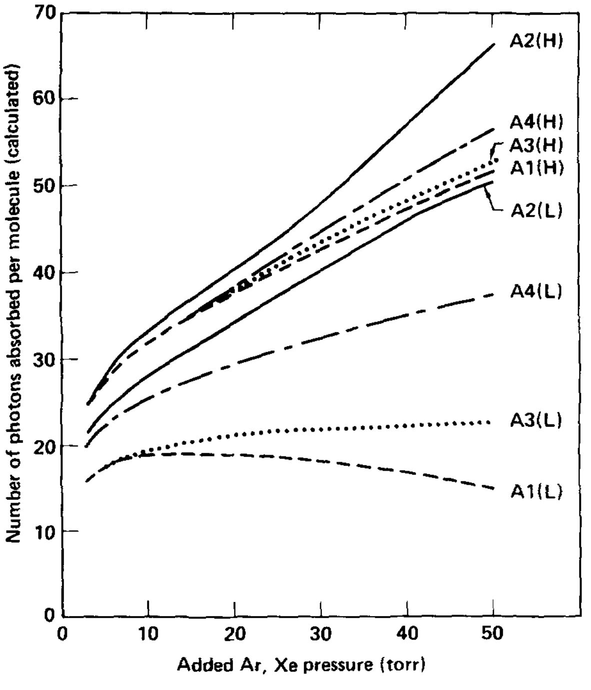

FIG. 6. Model predictions of the average number of photons absorbed per $CTCl_3$ molecule with added argon/xenon for both H: high fluence, 16 J/cm^2 and L: low fluence, 6 J/cm^2. Cases A1–A4 are further specified in the top part of Table I. (A1,- - - ; A2, —; A3,· · ·; A4, - - - - -).

The plots look very much alike for cases A1 and A3 in which $b = 0$ (the original absorption model) in each collision model. In comparison, there is relatively greater photon absorption in cases A2 and A4 with the alternate absorption model, in which the cross section decreases with increasing v. Comparing only these two $b = -0.79$ cases, many more net photons are removed from the laser beam with the original "k_{vib} = constant" vibrational relaxation model A2, than for A4. In general, the difference in photon absorption for the various models is most marked at high pressures and low fluences (6 J/cm^2). The uniquely large absorption cross section predicted by model A2 is thought to arise from the large number of collision deexcitation/reabsorption cycles that can occur in a molecule described by this model, with relatively minor concurrent changes of the population distribution at high v. In case A2, both $\sigma(v)$ and $k_{vib}(v)$ are large at low and intermediate v where ladder up-pumping is normally slowed anyway by rapid competitive stimulated emission.

To further examine this predicted behavior, a more extensive array of absorption/vibrational relaxation models was briefly surveyed. In each case the $CTCl_3$ harmonic vibrational ladder, Whitten-Rabinovitch level degeneracies and the RRKM unimolecular decay rates were employed. Rotational relaxation effects were removed by setting $x_F = 1.0$. Absorption models with $b = +0.75, 0, -0.75, -1.50$ were considered [*vis-a-vis* $b = 0$ (original) and $b = -0.79$ (alternate) above], along with a $k_{vib}(v) = c(v/v_d)^d$ dependence. A range of $d = +1.50, +0.75, 0, -0.75$ was chosen [*vis-a-vis* $d = 0$ (original) and $d = +1.0$ (alternate) above]. The parameter a in the absorption model [Eq. (6)] was adjusted so that at 10 J/cm^2 the local dissociation probability is 0.4 at zero pressure. For each a, b, and d-defining model, values of the collisional parameter c were determined to simulate a decrease in the 10 J/cm^2 fluence dissociation probability with 20 Torr added buffer down to either 0.25 (slow quenching) or 0.05 (fast).

Plots of photon absorption vs buffer pressure for the seven examined representative members of the b, d array are presented in Fig. 7 for the fast quenching regime, along with a schematic representation of $\sigma(v)$ and $k_{vib}(v)$ for each example presented. They are further identified as cases B1–B7 in the lower part of Table I. The "slow quenching" plots from 0 to 50 Torr (not shown here) closely follow the respective "fast quenching" curves in Fig. 7 compressed to the 0–15 Torr range. In the seven cases studied, $c[= k_{vib}(v_d)]$ for the fast quenching case is $3.74 \pm 0.16\times$ that obtained assuming the slow quenching condition.

As for $CTCl_3$ above (Fig. 6), this somewhat more general examination suggests that when the dissociation probability is fixed and the collision dynamics model is varied,

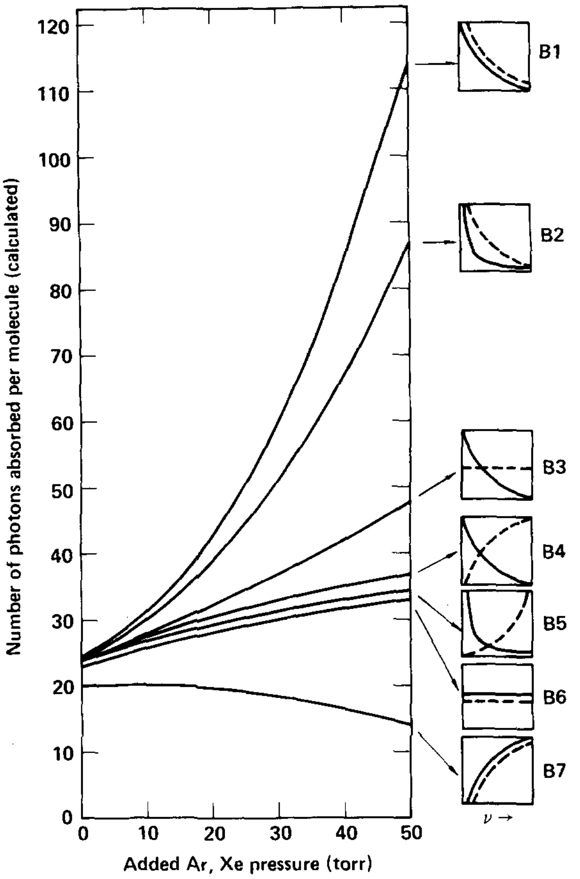

FIG. 7. Model predictions of the average number of photons absorbed per test molecule with added argon/xenon at 10 J/cm^2 fluence. The specific cases B1–B7 are detailed in Table I and the text. Next to each curve is the representative schematic of absorption $\sigma(v)$ (continuous lines) or collisional relaxation $k_{\text{vib}}(v)$ (dashed lines) vs the vibrational level v.

photon absorption is greatest when the absorption cross section and collisional relaxation constant are both large or largest at low vibrational energies, as in cases B1 and B2. The plots in Fig. 7 are for 10 J/cm^2 fluence. Other simulations (not exhibited in this figure) suggests that at lower fluences, where absorption experiments are more easily performed, the different predictions of these absorption/collision models are even more distinguished from one another, as was also found to be true in the $CTCl_3$ calculations (Fig. 6).

Photon absorption cross section and isotopic selectivity

Figure 2 shows that $CTCl_3$ selectively absorbs radiation near the 12 μ $\nu_4 \leftarrow 0$ peak (835 cm^{-1}) where $CDCl_3$ is highly transparent. The fluence-dependent and pulse-averaged absorption cross section of σ_T and σ_D for $CTCl_3$ and $CDCl_3$, respectively, can be related to the isotopic absorption selectivity $S = \sigma_T/\sigma_D$. Previously,[1] the low fluence value of S was measured to be $12\,000^{+\infty}_{-3000}$ at 835 cm^{-1} (the peak of $\nu_4 \leftarrow 0$ absorption) and $6500^{+\infty}_{-1900}$ at 828 cm^{-1} (near the peak of one frequency MPD). This result was based on a $CTCl_3$ ground state absorption cross section of 3.2×10^{-18} cm^2 at 835 cm^{-1} and 1.6×10^{-18} cm^2 at 828 cm^{-1}, coupled with an upper limit of the $CDCl_3$ absorption cross section as measured with an infrared spectrometer. Because of decreased excited state oscillator strength and saturated absorption in the multilevel absorption and dissociation processes, the net $CTCl_3$ absorption cross section at the saturation fluence ($\phi_{\text{sat}} \sim 20$ J/cm^2) is much smaller than this low-fluence value. Based on the absorption of 30 (12 μ) photons[1] at 20 J/cm^2 (828 cm^{-1}), the calculated net high-fluence $CTCl_3$ cross section is $\sigma_T(\phi_{\text{sat}}) \sim 2\times10^{-20}$ cm^2. A more useful measure of the optical selectivity, i.e., at the saturation fluence, can be derived from this new $CTCl_3$ cross section and more precise $CDCl_3$ absorption measurements.

The first set of absorption measurement data was taken with a sample from a bottle of 99.6% D $CDCl_3$ (0.4% $CHCl_3$) that had been opened 14 months. (The $CDCl_3$ used here has no added methanol to remove phosgene, an oxidation product.) An average absorption cross section of 3.8×10^{-22} cm^2 was obtained. This is about equal to the upper limit estimate obtained from the infrared spectrometer measurements. Additional runs were made with a freshly opened sample of 99.96% D $CDCl_3$. In the first run (at 110.8 Torr) the absorption coefficient was much smaller than before, 4.7×10^{-23} cm^2. The next run (at 191 Torr) gave 9.4×10^{-24} cm^2. For 50 Torr samples (assuming there is no pressure-broadened wing absorption) these two runs correspond to a 138 and 635 m $1/e$ absorption length and a 430 and 2100 high fluence T/D absorption selectivity, respectively. These high fluence T/D optical selectivities are sufficiently high for practical tritium recovery. Furthermore, these new measurements correspond to low fluence T/D absorption selectivities of 34 000 and 170 000 at 828 cm^{-1}. Subsequent infrared spectrometer measurements of neat $CHCl_3$ have shown that the stated 0.4% $CHCl_3$ contribution was far too small to account for the high earlier measured cross sections. Therefore, in practical applications of tritium recovery, impurities due to oxidation and room-lighting photochemistry of chloroform may, in fact, determine the background absorption and consequently must be minimized.

Isotopic selectivity in dissociation

The single step T/D enrichment factor (β) is defined here as the quotient of the dissociation probability of $CTCl_3$ per pulse (P_T) to that of $CDCl_3$ (P_D), $\beta = P_T/P_D$. Initial measurements[1] of the enrichment factor in dilute $CTCl_3/CDCl_3$ mixtures ($\eta = 200$ ppm) indicated a modest lower-limit value of 165. Since those initial measurements, the fundamental design of the photolytic system has been modified and upgraded, significantly reducing the random run to run nonreproducibility to $<0.2\%$. These improvements in the experimental apparatus enabled much more precise measurements of the single-step T/D enrichment factor, which in most cases is still characterized by lower limit bounds because of the difficulty in measuring very small values of P_D. Experiments were conducted to examine any possible contributions to P_D, and hence loss of isotopic selectivity, arising from direct 12 μ MPD of cold $CDCl_3$ [reaction (2), for which P_D is independent of the $CTCl_3$ partial pressure p_T], from 12 μ MPD of $CDCl_3$ which has been collisionally excited by $CTCl_3$ [reaction (4)], and from $CDCl_3$ decomposition by reaction with $CTCl_3$ MPD fragments [reaction (5)]. $P_D \propto p_T$ for the last two cases. For the presentation below, it is found to be convenient to separately consider the contributions to $CDCl_3$ decomposition by reactions (2), (4), and (5) as follows:

$$P_D = P_D^{(2)} + p_T[P_D^{(4)} + P_D^{(5)}], \tag{10}$$

so

$$\beta \equiv \frac{p_T}{P_D^{(2)} + p_T[P_D^{(4)} + P_D^{(5)}]} . \tag{11}$$

Equation (10) is correct only if $P_D^{(2)}, p_T P_D^{(4)}, p_T P_D^{(5)} \ll 1$, as is the case in these experiments. Note that $P_D^{(4)}$ and $P_D^{(5)}$ do not have the units of probability.

Figure 8 shows the results of several enrichment runs under various buffer gas conditions. In no case was there any evidence of $CDCl_3$ loss, within statistical limits. Though these conditions were not tailored to determine the highest lower bound of β, several interesting effects are observed. First, using 200 mTorr of $CDCl_3$, containing 200 ppm T/D without buffer, the logarithmic depletion plot is decidedly curved. A curvature in a first order decay plot is indicative of complicating secondary reactions, which in this case suggests that some $CTCl_3$ is being reformed following the initial photolytic step. Relatively small amounts of inert buffer gas returns the log depletion plot to straight line behavior. A complementary set of experiments was conducted utilizing analogous CO_2 laser photolysis of $CDCl_3$ ($\nu_4 \leftarrow 0$) at 10.91 μ offers the following observations and possible explanation of this behavior.

Photolysis of low pressure (200 mTorr) neat $CDCl_3$ also exhibits curved decay plots; whereas at higher pressure with either > 2 Torr of $CDCl_3$ or with added argon, the log decay plots become linear. Also, with a sufficient number of laser pulses, these low pressure run plots approach a limiting depletion value. Using gas chromatograph/mass spectrometer analysis of the residual $CDCl_3$ following photolysis of 200 mTorr neat samples, evidence of significant D/H exchange in the chloroform (~40% H/60% D) was found. No exchange was observed in null, nonlaser runs performed before or after the laser runs. Furthermore, similar MPD experiments using 2 Torr of neat $CDCl_3$ showed no hydrogen exchange, at similar fractional conversion. The initial step in chloroform photolysis has been shown to be production of DCl (TCl) and $:CCl_2$.[3] In the case of low pressure $CDCl_3$ photolysis, the DCl formed most likely goes to the walls and slowly exchanges to become partially protonated. Similarly, $:CCl_2$ produced from subsequent laser pulses can go to the walls at lower pressures, and react with the adsorbed HCl/DCl to reform $CHCl_3$/$CDCl_3$. As the total pressure is increased, the nascent $:CCl_2$ diffuses slower and now preferentially reacts with either itself or with parent $CDCl_3$, which results in less protonated parent being reformed. The presence of reactive proton sites on the wall of the photolytic cell is further evidenced by observation of (protonated) C_2HCl_3 and C_2HCl_5 products from neat $CDCl_3$ and neat C_2Cl_4 IRMPD.[4] An analogous mechanism may be important in the 12 μ $CTCl_3$ studies. In the T/D case, TCl is adsorbed on the walls and can reform $CTCl_3$ by reaction with $:CCl_2$ radicals. However, due to the large difference in $CTCl_3$ vs $CDCl_3$ concentration, plots of depletion of $CTCl_3$ will not reach a limiting value at low pressure.

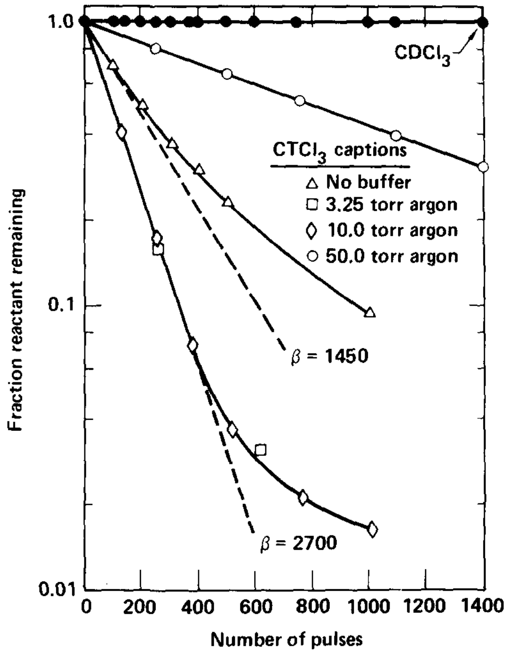

FIG. 8. The fraction of $CTCl_3$ and $CDCl_3$ reagent remaining after a variable number of incident laser pulses (200 ppm T/D, 200 mTorr chloroform; 12.08 μ, 380 mJ, 1.2 μs; 50 cm focal length lens). The $CDCl_3$ data is a compilation of all the displayed $CTCl_3$ conditions. The determined lower limit of the single step enrichment factor β is labeled on each curve.

Addition of 10 Torr of argon buffer to the T/D chloroform mixture results in a linear log depletion plot with 12 μ irradiation, and a larger β value of 2700 compared with the unbuffered limiting value of 1450 (Fig. 8). This larger enrichment factor is due to the collision-induced increase in the $CTCl_3$ dissociation probability. The small, MPA rotational bottleneck is removed by hole-filling collisions with either chloroform or inert buffer as described above (Figs. 4 and 5).

A consistent secondary change in slope occurs at very high depletion levels as shown in Fig. 8. Runs made using 3.25 Torr of added argon [the pressure at which the dissociation probability per pulse equals that with 10 Torr argon (Fig. 5)], indicates that this phenomenon is not due to a diffusion process, as was the case with no buffer. With further increase of the buffer gas (or chloroform) pressure, vibrational deactivation eventually competes with rotational hole filling, and then P_T and the enrichment factor both decrease as shown by the 50 Torr argon result (Fig. 8). The observation of the secondary reduction in slope occurring at high depletion in several long irradiation experiments, suggests that the remaining chloroform is $^{13}CTCl_3$ (natural abundance of 1.1%), since it was never possible to deplete greater than ~99% of the $CTCl_3$. Because the width of the MPD $^{12}CTCl_3$ frequency profile is ~16 cm^{-1} (FWHM—Fig. 2), the $^{13}CTCl_3$ isotope shift must be of at least this magnitude to have a suitably small MPD probability at 12.08 μ. Figure 9 shows that the depletion fraction only drops from 7% to ~1% as the number of laser pulses increases from 100 to 3200. This represents a decrease in dissociation probability on the order of 100.

To investigate the possible contribution of $^{13}CTCl_3$ to this observed behavior, the band center frequencies for

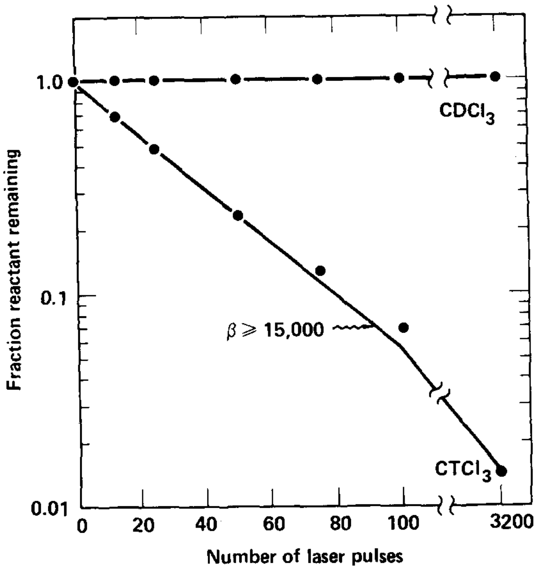

FIG. 9. The fraction of $CTCl_3$ or $CDCl_3$ remaining after irradiation obtained with more precise measurement of $CDCl_3$ loss *vis-a-vis* the experiments displayed in Fig. 8, employing optimized conditions (240 ppm T/D, 200 mTorr chloroform in 5 Torr argon, 12.08 μ, ~1.3 J/pulse, 50 cm focal length lens with 1 pass retroreflection).

$^{13}CHCl_3$, $^{13}CDCl_3$, and $^{13}CTCl_3$ were calculated using the Wilson *F-G* matrix method,[21] and the general harmonic force field for $^{12}CTCl_3$ from Ref. 22, as described previously for CTF_3 [23] and C-12 chloroform.[1] The calculated ν_4, $\nu_5 \leftarrow 0$ absorption peaks are shown in Table II for each of the ^{35}Cl, H/D/T chloroform species. As previously noted,[1] these earlier calculations are in quite good agreement with observations. [Note that the large spectral shift in ν_5 for $CHCl_3$ (^{13}C–^{12}C) corresponds to the ν_4 spectral shift in $CTCl_3$.]

The calculated $^{12}CTCl_3$ $\nu_4 \leftarrow 0$ peak frequency is very close to the measured value. [The ν_4 ^{37}Cl isotope shift is small, ($^{12}CT^{35}Cl_3 - {}^{12}CT^{37}Cl_3) = 1.6$ cm^{-1}.] The absorption frequency for $^{13}CTCl_3$ is calculated to be 812.8 cm^{-1}, after suitably shifting for the difference in calculated and observed $^{12}CTCl_3$ vibrational frequency (not shown in Table II). Furthermore, the peak $^{13}CTCl_3$ MPD frequency should be at 806 cm^{-1}, again assuming the same shift as in $^{12}CTCl_3$.

At the 828 cm^{-1} laser frequency, the dissociation yield for $^{13}CTCl_3$ should be near zero under the photolysis conditions shown in Fig. 2, because it should have the same MPD probability as $^{12}CTCl_3$ at 850 cm^{-1}. Therefore, photolysis of $CTCl_3$ at 828 cm^{-1} eventually depletes the $^{12}CTCl_3$ isotope resulting in a 1% residual $^{13}CTCl_3$ fraction, which is too far off resonance to dissociate much.

By choosing the optimal buffer gas pressure (Fig. 5) and maximizing the pulse energy (using multipass retroreflection) to maximize the cell-averaged P_T, an optimized enrichment factor was obtained. The results of this experiment are shown in Fig. 9 ($\eta = 200$ ppm). With 3200 pulses incident, ~0.6% $CDCl_3$ apparently was lost, compared to ~0.4% loss in a null run (laser off, gas mixture in cell for the time equivalent to 3200 pulses). Though this suggests a net ~0.2% loss of $CDCl_3$, the conservative estimate of $\beta \geq 15\,000$ was made using the 0.6% loss uncorrected datum point. (Using the corrected value results in $\beta \geq 45\,000$.) Note that this experiment also shows the change in slope at high depletion levels, now attributed to residual $^{13}CTCl_3$.

The above-described enrichment experiments are most sensitive to collision-free direct 12 μ MPD of $CDCl_3$ and therefore provide a relatively good measurement of $P_D^{(2)}$ and $\beta(\eta = 0)$. They are less sensitive to $CTCl_3$-related mechanisms of $CDCl_3$ decomposition, reactions (4) and (5), because of the rapid loss of $CTCl_3$ in the cell after even a few irradiation pulses and because of the small initial T/D ratios η. Consequently, $CTCl_3$-related $CDCl_3$ dissociation was more preferentially examined by irradiating a 1% T/D mixture of chloroform (500 mTorr) with 375 mJ, 12.08 μ laser radiation (1500 pulses). In the previous experiments, the magnitude of the gas chromatograph chloroform effluent concentration (> 99.99% $CDCl_3$) was monitored by thermal conductivity, and the usually much lower (~200 ppm) level of $CTCl_3$ required detection by the ionization chamber which follows the thermal conductivity detector. However, with such high (1%) T/D ratios, the $CTCl_3$ concentration could be monitored by both detectors in this case. In this irradiation experiment, essentially all (> 98%) $CTCl_3$ was removed, as monitored by the ionization chamber, and there was a ~1.5 ± 0.2% loss in the total chloroform product as mea-

TABLE II. Fundamental frequencies in chloroform (CH $^{35}Cl_3$).

		Calculated		(^{12}C-^{13}C)	
	Observed[a]	^{12}C	^{13}C	Calculated	Observed
ν_4					
$CHCl_3$	1219.7	1223.6	1221.2	2.4	2.6[b]
$CDCl_3$	914.5	913.0	902.7	10.3	N/A[f]
$CTCl_3$	835.3	837.1	814.6	22.5	N/A
ν_5					
$CHCl_3$	773.1[c]	777.6	753.2	24.4	23.2[d]
$CDCl_3$	747[e]	746.2	729.5	16.7	N/A
$CTCl_3$	674	673.0	668.5	4.5	N/A

[a] Frequencies are in cm^{-1}, $^{12}CHCl_3$ (Ref. 24), $^{12}CDCl_3$ (Ref. 22), $^{12}CTCl_3$ (Ref. 1).
[b] Reference 24.
[c] ±0.5 cm^{-1}.
[d] ±1 cm^{-1}.
[e] ±2 cm^{-1}.
[f] N/A: Not available.

sured by the thermal conductivity detector. Within the accuracy of this experiment, for every $CTCl_3$ molecule removed by 12 μ MPD, apparently 0.5 ± 0.2 $CDCl_3$ was also lost.

Using the $CDCl_3$ dissociation mechanism described by reactions (1)–(5) and Eq. (10), and the experimental relation $pP_D = 0.5 p_T P_T$ (where p = chloroform partial pressure and η is assumed to be $\ll 1$), for this particular experiment only:

$$P_D = P_D^{(2)} + p_T\left[P_D^{(4)} + P_D^{(5)}\right] \simeq 0.5 \eta P_T, \tag{12}$$

where $\eta = 10^{-2}$ and $p_T = 500$ mTorr $\times \eta$. The two extreme mechanistic possibilities for $CDCl_3$ consumption are $CTCl_3$-independent removal $[P_D^{(4)} + P_D^{(5)} = 0]$, for which $P_D^{(2)}/P_T \simeq 5 \times 10^{-3}$ here, and solely $CTCl_3$-dependent $CDCl_3$ decomposition $[P_D^{(2)} = 0]$, for which $[P_D^{(4)} + P_D^{(5)}]/P_T \simeq 1$/Torr. Since both routes may contribute to the mechanism, these P_D/P_T values are upper-limit estimates.

One may determine the analogous upper-limit P_D/P_T parameters for the experiments with $\eta = 200$ ppm/200 mTorr chloroform, for direct comparison with the above results. Such a comparison is reasonable because in both cases the same laser pulse width and fluence were used and the same local values of $P_T (P_T \sim 1$; independent of pressure in this regime) dominate the volume-averaged contributions to the observed dissociation probability. In this case the upper limit values are $P_D^{(2)}/P_T = 6.7 \times 10^{-5} [P_D^{(4)} + P_D^{(5)} = 0]$ and $[P_D^{(4)} + P_D^{(5)}]/P_T = 1.7$/Torr $[P_D^{(2)} = 0]$. The derived upper-limit values of $[P_D^{(4)} + P_D^{(5)}]/P_T$ are roughly the same whether determined from the $\eta = 200$ ppm or the $\eta = 10^{-2}$ data. However, the respective $P_D^{(2)}/P_T$ upper limits are not in agreement; the $\eta = 200$ ppm experiment sets a much more stringent upper limit for the $CDCl_3$ direct photolysis probability $[P_D^{(2)}/P_T]$. Therefore, any observed $CDCl_3$ loss in the $\eta = 10^{-2}$ experiment must be due to the $CTCl_3$ collision-induced dissociation of $CDCl_3$ [reaction (3) followed by reaction (4)] and/or reaction of $CTCl_3$ photolysis fragments ($:CCl_2$) with $CDCl_3$ [reaction (5)], and is not due to direct photolysis of cold $CDCl_3$. However, the relative contributions of these three reactions (2), (4), and (5), for the 200 ppm study are not clear. Still, these observations imply that there are few reactive encounters between chloroform molecules and the $CTCl_3$ dissociation products and, as such, are consistent with preliminary conclusions of $^{13}CHCl_3/^{12}CDCl_3$ isotope labeling studies.[5]

For a heavy water fission reactor tritium recovery plant with initial T/D fraction $\eta \sim 5$ ppm and chloroform $p = 20$ Torr, one may conclude that $\beta \geqslant 15\,000$ if reaction (2) dominates or $\beta \simeq 10\,000$ if $CTCl_3$-related collisions with $CDCl_3$ [reactions (4) and (5)] dominate. These estimates of the enrichment factor are based on the most stringent P_D/P_T parameters from the $\eta = 10^{-2}$ and 200 ppm experiments, and also assume $P_T \sim 1$, as above.

Clearly, there are several simplifying assumptions in the above analysis, aside from the additive form of Eq. (10). $P_D^{(2),(4),(5)}/P_T$ are functions of laser intensity and fluence, and the important tradeoffs between maximizing β vs P_T have also not been addressed. {Furthermore, the importance of a *high* T/D enrichment factor β to a practical process is not completely described in the working definition of β used here [Eq. (11)]. Loss of $CDCl_3$ by reactions (2), (4), and (5), and by nonselective mechanisms increase P_D and the chloroform feedstream make-up operating costs. However, each of these $CDCl_3$ loss reactions need not produce DCl, and therefore need not degrade the T/D fraction in the collected tritium chloride. For instance, reaction (5) and nonselective $CDCl_3$ losses (wall reactions, $CDCl_3$/TCl collection nonselectivity, etc.) probably produce deuterated chlorinated alkanes and perhaps little DCl.}

$CTCl_3/CDCl_3$ post-photolysis chemistry

The three-center DCl elimination was recently shown to be the dominant dissociation pathway ($\geqslant 99\%$) in the infrared photolysis of $CDCl_3$ in a molecular beam.[3] For tritiated chloroform, the analogous reaction:

$$CTCl_3 + nh\nu \rightarrow :CCl_2 + TCl \tag{1b}$$

occurs with same activation energy, ~ 62 kcal/mol. Following photolysis, the TCl is likely unreactive and can be immediately separated from the feedstream in closed-loop operation.[25] A discussion of the fate of the $:CCl_2$ radical has been detailed elsewhere.[5] Briefly, since the $:CCl_2$ concentration is very low ($\eta \sim 200$ ppm), the dominant removal mechanism is probably not by recombination with itself, but rather by the reaction with the bath of $CDCl_3$ to form C_2Cl_4 + DCl, even though the rate constant of dichlorocarbene removal by $:CCl_2 + :CCl_2$ is estimated[5] to be perhaps 100 times greater than that for reaction with $CDCl_3$. Based on this mechanism [reaction (5)], one obtains $pP_D = p_T P_T$ for $\eta \ll 1$, because one $CDCl_3$ molecule is consumed for each $CTCl_3$ photolyzed. This is reasonably consistent with the observation in the $\eta = 10^{-2}$ experiment that 0.5 ± 0.2 $CDCl_3$ molecules are lost per $CTCl_3$ dissociated.

Though the alternate route of $CTCl_3$ dissociation:

$$CTCl_3 + nh\nu \rightarrow \cdot CTCl_2 + Cl \tag{1c}$$

has a very small branching fraction, f, say $\sim 10^{-3}$–10^{-2} based on Ref. 3 (and dependent on the laser intensity and pulse width), it can strongly impact the post-photolysis chemistry and P_D if it leads to chain reactions with length $> 1/f$ (i.e., $1/f$ $CDCl_3$ consumed per $CTCl_3$).

For example, Cl from reaction (1c) can lead to

$$Cl + CDCl_3 \rightarrow \cdot CCl_3 + DCl, \quad \Delta H = -7.8 \text{ kcal/mol} \tag{13}$$

and further chemistry. The most exothermic reaction of the tritiated fragment from reaction (1c) with bulk $CDCl_3$ involves formation of a tritiated alkane plus a chlorine atom (14a). If the bulk $CDCl_3$ is sufficiently hot, further endothermic decomposition of this activated alkane is possible to form TCl or DCl (14b) and (14c). Even more endothermic reactions are the elimination of a tritium or deuterium atom (14d) and (14e) or elimination of a chlorine molecule (14f). Abstraction of a chlorine atom from $CDCl_3$ reforms $CTCl_3$ (15a), whereas abstraction of a deuterium atom is highly endothermic (15b). Reactions of $\cdot CTCl_2$ with itself are highly exothermic (16) but unlikely at low (ppm) concentrations. Another very likely possibility is that the $\cdot CTCl_2$ simply goes to the walls and either sticks or abstracts a proton to form $CHTCl_2$ (17).

$$\cdot CTCl_2 + CDCl_3 \rightarrow C_2DTCl_4 + Cl \quad -\ 8.3\ \text{kcal/mol} \tag{14a}$$

$$\rightarrow C_2DCl_3 + TCl + Cl \quad +\ 4.5 \tag{14b}$$

$$\rightarrow C_2TCl_3 + DCl + Cl \quad +\ 4.5 \tag{14c}$$

$$\rightarrow C_2TCl_5 + D \quad +13.1 \tag{14d}$$

$$\rightarrow C_2DCl_5 + T \quad +13.1 \tag{14e}$$

$$\rightarrow C_2DTCl_2 + Cl_2 + Cl \quad +27.1, \tag{14f}$$

$$\cdot CTCl_2 + CDCl_3 \rightarrow CTCl_3 + \cdot CDCl_2 \quad \sim 0 \tag{15a}$$

$$\rightarrow CDTCl_2 + \cdot CCl_3 \quad +42.9, \tag{15b}$$

$$\cdot CTCl_2 + \cdot CTCl_2 \overset{M}{\rightarrow} C_2T_2Cl_4 \quad -85.5 \tag{16a}$$

$$\rightarrow C_2TCl_3 + TCl \quad -73.0 \tag{16b}$$

$$\rightarrow C_2T_2Cl_2 + Cl_2 \quad -50.4, \tag{16c}$$

$$\cdot CTCl_2 + H(\text{wall}) \rightarrow CHTCl_2 \quad -52.3. \tag{17}$$

However, despite the possible reactions with $\Delta H < 0$, this reaction (1c)-based mechanism is still probably not important. At room temperature, reactions (13)–(17) apparently cannot support a chain with more than a few $CDCl_3$ lost per $CTCl_3$ (which is $\ll 1/f$ under any irradiation conditions of interest) because there is no exothermic or thermoneutral chain propagating step for the important radicals Cl, $\cdot CCl_3$, and $\cdot CDCl_2$. Since η is small, the medium remains cold during and after photolysis, and there is no thermal unimolecular dissociation of chloroalkanes to form Cl atoms. $\cdot CCl_3$ produced in reaction (13) could react with $CDCl_3$ endothermically ($\Delta H = +8.9$ kcal/mol) to form $\cdot CDCl_2$ and CCl_4. In addition, the chlorinated alkanes and alkenes produced in the possible $\cdot CDCl_2 \rightarrow Cl$ propagation steps [analogs of reactions (14)] are not observed in resonant 11 μ photolysis of $CDCl_3$.[5] Furthermore, even if the branching fraction to reaction (1c) were the estimated maximum, $f \sim 10^{-2}$, then there would be the possibility of detecting tritiated product (other than TCl), especially in runs utilizing large initial mole fractions of $CTCl_3$ ($\eta = 1\%$), and having large dissociation fractions. These products would also be easily identified since their appearance in the (extremely sensitive) ionization chamber signal would track their known gas chromatograph retention times. However, in no experiment was any tritiated product ever detected. This includes TCl which, as expected, either goes to the walls or is not eluted from the gas chromatograph. (Blank runs starting with large amounts of pure DCl in the cell never showed any thermal conductivity detector signal due to DCl, therefore confirming that observation of TCl photoproduct is not expected.) Still, in all cases deuterated/tritiated organics would be efficiently transferred and detected if present.

CONCLUDING REMARKS

The 12 μ infrared multiple-photon dissociation of $CTCl_3$ has been investigated in regard to wavelength dependence, effect of collisions with inert gas and chloroform molecules, and absorption and dissociation T/D selectivity. The single frequency wavelength dependence of $CTCl_3$ MPD in the ν_4 absorption band was found to peak $\sim 10\ \text{cm}^{-1}$ to the red of the absorption peak at 835 cm^{-1}, consistent with the $CTCl_3$ ν_4 mode anharmonicity ($X_{44} = -8.9\ \text{cm}^{-1}$).

The effect of inert gas and chloroform collisions with activated $CTCl_3$ molecules was investigated and modeled, using an energy-grained, master equation formalism. Best fit behavior was obtained by assuming an absorption cross section and a vibrational deactivation rate constant independent of vibrational level. Employing this simple vibrational-independent model resulted in rapid ground vibrational state rotational relaxation rate constant (k_{rot}) of 1.2×10^{-10} cm^3/molecule s (300 K), for He, Ar, and Xe. This value corresponds to $CTCl_3$-rare gas collision cross sections of 9.4, 26, and 38 Å^2 for He, Ar, and Xe, respectively, which are only somewhat smaller than gas kinetic. The vibrational relaxation constant (k_{vib}) which best fits the data is somewhat smaller (than k_{rot}) for Ar and Xe, $k_{\text{vib}} \sim 2.5 \times 10^{-11}$ cm^3/molecule s, and smaller still for He, $k_{\text{vib}} \sim 3.8 \times 10^{-11}$ cm^3/molecule s. These values translate to a $CTCl_3$ vibrational energy loss of 50, 70, and 90 cm^{-1} per collision, for He, Ar, and Xe. As expected, k_{vib} for $CTCl_3/CDCl_3$ encounters is considerably greater and a best fit value of $\sim 1100\ \text{cm}^{-1}$ lost per collision was found.

The vibrational level-independent absorption cross section and relaxation rate constant models used here do not provide a unique fit, as models with decreasing absorption cross section and/or increasing relaxation rate constant with v also provided good simulations. In each fit, the relaxation rate constant for levels near the dissociation energy varied within a narrow range of values ($\pm 25\%$). For the case of the $CTCl_3$ simulation, each model has a specific, distinctive absorption cross section as a function of fluence and buffer pressure. Greatest photon absorption occurs in models with large absorption and fast relaxation peaking at low and intermediate values of v in the vibrational ladder. This observation was "extended" to more general molecules in a brief continuation of this study.

Such modeling of photon absorption is important in isotope separation for two reasons. Photon extraction from the laser beam beyond the minimum dissociation requirements is undesirable. However, such excess absorption by the minority, to-be-separated isotope is usually trivial in practice. More importantly, when energy is transferred to the majority isotope (reaction 3), significant photon absorption and nonselective dissociation can occur (reaction 4).

The T/D isotopic absorption selectivity for $CTCl_3$ was remeasured using long path laser transmission, resulting in very large values exceeding 34 000. This selectivity remains much greater than 500 even near the saturation fluence (~ 15 J/cm) at 828 cm^{-1}. The $CTCl_3$ dissociation probability per pulse was remeasured under refined experimental conditions and a conservative lower limit single step enrichment factor of $> 15\,000$ at 828 cm^{-1} was obtained; a more optimistic value of 45 000 can be supported by statistical experimental dynamic range considerations.

Preliminary two-frequency MPD experiments have been performed and were reported in Refs. 5 and 26; more refined measurements are currently underway. Also work is continuing to develop a higher efficiency laser source for $CTCl_3$ MPD employing rotational Raman scattering in either D_2, HD, or NH_3.[26]

ACKNOWLEDGMENTS

The authors wish to acknowledge the excellent technical assistance of Virgil Duval, who helped conduct most of the experimental work, and Larry Walkley and William Miller for design and construction of the experimental apparatus. We also wish to thank Dr. Frederick Aldridge for helpful comments regarding this work, Dr. Jon Maienschein for several valuable discussions and a critical reading of this manuscript, and Clyde Griffith and other members of the LLNL Tritium Facility for their aid in the synthesis of tritiated compounds. This work performed under the auspices of the U. S. Department of Energy by the Lawrence Livermore National Laboratory under contract number W-7405-ENG-48.

[1] F. Magnotta, I. P. Herman, and F. T. Aldridge, Chem. Phys. Lett. **92**, 600 (1982).
[2] Y. Makide, S. Kato, T. Tominaga, and K. Takeuchi, Appl. Phys. B **32**, 33 (1983).
[3] I. P. Herman, F. Magnotta, R. J. Buss, and Y. T. Lee, J. Chem. Phys. **79**, 1789 (1983).
[4] F. T. Aldridge, I. P. Herman, F. Magnotta, and J. L. Maienschein, Lawrence Livermore National Laboratory, Livermore, CA, UCID-18509-82-3, 4-83-1,2 (August 1983), unpublished, available from NTIS.
[5] I. P. Herman, F. Magnotta, and F. T. Aldridge, Isr. J. Chem. (in press).
[6] B. T. Darling and D. M. Dennison, Phys. Rev. **57**, 128 (1940).
[7] M. V. Garcia, R. Escribano, G. Del Rio and J. M. Orza, An. Quim. **71**, 745 (1975).
[8] J. R. Barker, J. Chem. Phys. **72**, 3686 (1980).
[9] P. J. Robinson and K. A. Holbrook, *Unimolecular Reactions* (Wiley-Interscience, New York, 1972), p. 131.
[10] S. Ruhman and Y. Haas, J. Chem. Phys. **76**, 1317 (1982).
[11] A. C. Hindmarsh, Lawrence Livermore National Laboratory, Livermore, CA, UCID-30001-82, Rev. 1 (1972), unpublished, available from NTIS.
[12] V. T. Platonenko, JETP Lett. **25**, 46 (1977); Sov. J. Quantum Electron. **8**, 1010 (1978).
[13] W. Fuss and K. L. Kompa, Prog. Quantum Electron. **7**, 117 (1981).
[14] See, e.g., I. P. Herman and J. B. Marling, Chem. Phys. Lett. **64**, 75 (1979); C. R. Quick, Jr. and C. Wittig, J. Chem. Phys. **69**, 4201 (1978).
[15] J. E. Eberhardt, R. B. Knott, A. W. Pryor, and R. G. Gilbert, Chem. Phys. **69**, 45 (1982); H. L. Dai, Chem. Phys. Lett. **96**, 324 (1983); M. V. Kuzmin and A. A. Stuchebrukhov, Chem. Phys. **83**, 115 (1984).
[16] M. J. Rossi, J. R. Pladziewicz, and J. R. Barker, J. Chem. Phys. **78**, 6695 (1983).
[17] H. Hippler, J. Troe, and H. J. Wendelken, J. Chem. Phys. **78**, 6709, 6718 (1983).
[18] S. E. Schwartz and H. S. Johnston, J. Chem. Phys. **51**, 1286 (1969).
[19] J. O. Hirschfelder, C. F. Curtiss, and R. B. Bird, *Molecular Theory of Gases and Liquids* (Wiley, New York, 1954).
[20] G. A. Miller and R. B. Bernstein, J. Phys. Chem. **63**, 710 (1959).
[21] E. B. Wilson, Jr., J. C. Decius, and P. C. Cross, *Molecular Vibrations* (McGraw-Hill, New York, 1955).
[22] A. Ruoff and H. Burger, Spectrochim. Acta Part A 26, 989 (1970).
[23] I. P. Herman and J. B. Marling, J. Phys. Chem. **85**, 493 (1981).
[24] K. H. Schmidt and A. Muller, J. Mol. Spectrosc. **50**, 115 (1974).
[25] J. L. Maienschein, F. Magnotta, I. P. Herman, F. T. Aldridge, and P. Hsiao, Nucl. Tech./Fusion **4**, 121 (1983).
[26] F. Magnotta, I. P. Herman, F. T. Aldridge, and J. L. Maienschein, *Proc. Intl. Conf. Lasers 1983* (STS, McLean, VA, 1984).